Research Article

applied optics

Hybrid optical imaging with near-infrared, mid-infrared, and terahertz wavelengths for nondestructive inspection [Invited]

YU TOKIZANE,[1] HIKARU EJIRI,[2] TAKEO MINAMIKAWA,[1] SAFUMI SUZUKI,[3] MASAHIRO ASADA,[4] AND TAKESHI YASUI[1,*]

[1]*Institute of Post-LED Photonics (pLED), Tokushima University, 2-1 Minami-Josanjima, Tokushima, Tokushima 770-8506, Japan*
[2]*Faculty of Science and Technology, Tokushima University, 2-1 Minami-Josanjima, Tokushima, Tokushima 770-8506, Japan*
[3]*Graduate School of Science and Engineering, Tokyo Institute of Technology, 2-12-1 Ookayama, Meguro, Tokyo 152-8552, Japan*
[4]*Institute of Innovative Research, Tokyo Institute of Technology, 2-12-1 Ookayama, Meguro, Tokyo 152-8552, Japan*
Corresponding author: yasui.takeshi@tokushima-u.ac.jp

Optical imaging is a powerful tool for nondestructive inspection, with high spatial resolution and low invasiveness. As light–material interactions vary a great deal depending on the wavelength, it is difficult to select the best imaging wavelength without prior knowledge of the optical properties of the material. To overcome this difficulty, we constructed a hybrid optical imaging system using three different wavelengths: near-infrared (NIR), mid-infrared (MIR), and terahertz (THz) regions. The same imaging optics were integrated with different light sources and detectors. Depending on the light–material interaction and detection sensitivity, NIR and THz imaging indicated some potential for nondestructive inspection, but MIR imaging showed difficulty. A combination of NIR and THz imaging will be a powerful tool for optical nondestructive inspection.   © 2021 Optical Society of America

1. INTRODUCTION

Nondestructive inspection [1] is a powerful tool for examining defects in industrial products, ensuring their safety and reliability. Conventionally, x rays [2,3] and ultrasound [4,5] have been widely used for nondestructive inspection. X rays have excellent material penetration but high invasiveness to the human body, leading to health problems, because its high photon energy (typically, $0.1 \sim 100$ keV) causes photoionization of cells. Also, the excessively high transmission often hampers obtaining good image contrast in nonmetal materials such as plastics, rubber, and ceramics. On the other hand, ultrasound has good penetration and low invasiveness; however, ultrasound testing cannot be used for remote sensing due to the large attenuation of ultrasound in air. Also, the limited spatial resolution is another problem with ultrasound imaging.

Optical imaging is another modality for nondestructive inspection with low invasiveness and high spatial resolution, covering a wide range of wavelengths from visible to infrared (IR), and terahertz (THz) waves. Invasiveness of these wavelengths is significantly lower than that of x-ray because of low photon energy: typically, >1000 meV for visible light, 10–1000 meV for infrared light, and 1–10 meV for THz waves. Since materials have a wide variety of interactions with optical waves depending on the wavelength, the probing capability and penetration power differ depending on the wavelength. Also, the spatial resolution depends on the wavelength due to the diffraction limit. Unfortunately, as visible light has low penetration power due to large absorption and/or scattering regardless of the submicrometer spatial resolution, its use for nondestructive inspection is limited to the surfaces of industrial products. Infrared light has sensitivity to molecular vibrations [6] as well as better penetration power than the visible light. More specifically, near-infrared light (NIR light, wavelength = 0.8–2.5 μm) is sensitive to the overtones of molecular vibrations, and benefits from the availability of mature lights sources and detectors. A combination of NIR imaging and spectroscopic analysis is used for nondestructive analysis of biological materials [7] and foods [8]. Mid-infrared light (MIR light, wavelength = 2.5–30 μm) is more sensitive to molecular vibrations due to its fundamental tones and interacts with the rich MIR spectral fingerprints of materials. Therefore, MIR imaging has been used for examining drug–polymer blends [9] and biological tissues [10]. More recently, THz waves have appeared as a new imaging modality for nondestructive inspection due to the moderate penetration in nonmetal, nonpolar materials, low invasiveness, and unique THz spectral fingerprints [11,12]. THz imaging has been effectively applied for nondestructive inspection of reinforced

plastics [13], ceramics [14], wood [15], illegal drugs [16], and cultural heritage [17].

Conventionally, imaging systems in NIR, MIR, and THz regions have been well established as an independent system and have been individually employed for investigation of objects with known optical properties. However, if a material has entirely unknown optical properties, it is not necessarily so easy to select the suitable imaging wavelength. To guess the suitable imaging wavelength prior to the practical imaging, a hybrid optical imaging system capable of covering wavelengths from NIR to MIR and THz regions would be a powerful tool. Based on the guess, one can select the practical imaging system in the NIR, MIR, or THz region. However, there have been no attempts to develop such a hybrid optical imaging system. In this article, we have integrated NIR imaging, MIR imaging, and THz imaging systems to construct a hybrid NIR/MIR/THz imaging system by using the same imaging optics with different light sources and detectors. We then demonstrated its effectiveness in nondestructive inspection of nonmetal objects.

2. EXPERIMENTAL SETUP

Figure 1 shows the experimental setup of the hybrid NIR/MIR/THz imaging system. We prepared three kinds of light sources with three largely different wavelengths: an NIR external cavity laser diode (NIR-ECLD; RIO, Santa Clara, CA, U.S.; Colorado, RIO-03235-5-04-0, wavelength = 1527.6–1565.6 nm, power = 20 mW), an MIR quantum cascade laser (MIR-QCL; DRS Daylight Solutions, San Diego, CA, U.S.; MIRCAT-QT-2100, wavelength = 6–11 µm, power <300 mW), and a THz resonant tunneling diode [18,19] (THz-RTD; wavelength = 698 µm, frequency = 0.430 THz, power = 2.3 µW). The laser beam used for imaging was selected by flip mirrors (FMs). The selected laser beam was focused onto a sample with an off-axis parabolic mirror (OAPM1; focal length = 75 mm), and was then collimated by another off-axis parabolic mirror (OAPM2; focal length = 75 mm) after passing through the sample. We prepared three kinds of detectors with sensitivities to different wavelengths: an NIR InGaAs-photodetector (NIR-PD; Electro-Optics Technology, Inc., Traverse, MI, U.S.; ET-3020, wavelength sensitivity = 950–1650 nm, frequency response <2.5 MHz), an MIR thermal power meter (MIR-PM; Thorlabs Inc., Newton, NJ, U.S.; S425C, wavelength sensitivity = 190 nm–20 µm, response time
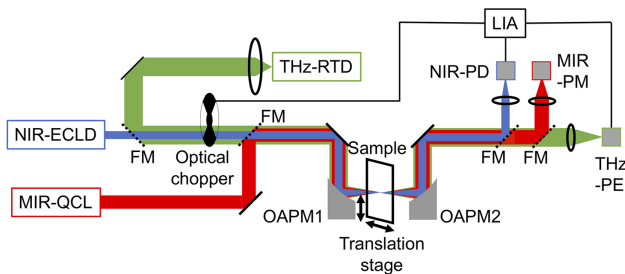
Fig. 1. Experimental setup. NIR-ECLD, NIR external cavity laser diode; MIR-QCL, MIR quantum cascade laser; THz-RTD, THz resonant tunneling diode; FMs, flip mirrors; OAPM1 and OAPM2, off-axis parabolic mirrors; NIR-PD, NIR InGaAs photodetector; MIR-PM, MIR thermal power meter; THz-PE, THz pyroelectric detector; LIA, lock-in amplifier.

= 0.6 s), and a THz pyroelectric detector (THz-PE; PHLUXi, Inc., Harumi, Tokyo, Japan; PYD-1, wavelength sensitivity = NIR–300 µm, frequency response <300 Hz). A lock-in amplifier (LIA; NF Corporation, Yokohama, Japan; LI5640, frequency range <100 kHz) was adopted to achieve good a signal-to-noise ratio (SNR) in THz imaging and NIR imaging. Unfortunately, the slow response of the MIR-PM prevented us from adopting lock-in detection in MIR imaging. For imaging measurement, the lateral position of the sample was linearly raster-scanned by using a translational stage (SURUGA SEIKI Co., Ltd., Shizuoka, Shizuoka, Japan; K161-85, travel length = 80 mm, travel step = 2 µm).

3. RESULTS

A. Imaging Performance

To evaluate the spatial resolution of the hybrid NIR/MIR/THz imaging system, we perform knife-edge measurements using a razor blade at three different wavelengths: $\lambda_{NIR} = 1.6$ µm for NIR imaging, $\lambda_{MIR} = 6.3$ µm for MIR imaging, and $\lambda_{THz} = 698$ µm for THz imaging. Figure 2 shows the result of the knife-edge measurements in (a) NIR imaging, (b) MIR imaging, and (c) THz imaging. The dependence of the knife-edge profile on the wavelength can be clearly confirmed. From curve fitting analysis with an error function, we determined the focal spot size: 43 µm for NIR imaging, 94 µm for MIR imaging, and 1104 µm for THz imaging, as shown in Fig. 2(d). Table 1 shows the comparison of focal spot size between the experimental and theoretical values in NIR, MIR, and THz imaging. The experimental value of the spatial resolution was in moderate agreement with the theoretical value, indicating imaging performance close to the diffraction limit. There is room for improvement of spatial resolution by using an optical beam with a larger diameter and/or an OAPM1 with a shorter focal length.

We next investigated a dynamic range (DR) of optical intensity measurement in NIR, MIR, and THz imaging, which is defined as a ratio of a mean of signal to that of noise. The resulting DR was 5177 in NIR imaging (LIA time constant = 100 ms), 55 in MIR imaging (number of signal accumulation = 100), and 68 in THz imaging (LIA time constant = 100 ms). We also investigated an SNR of optical intensity in the same system. When SNR is defined as a ratio of a mean to a standard deviation of signal, the resulting SNR was 3976 in NIR imaging (LIA time constant = 100 ms), 341 in MIR imaging (number of signal accumulations = 100), and 81 in THz imaging (LIA time constant = 100 ms). Although the averaging effect of the acquired signal was different among those imaging systems, moderate DR and SNR were achieved. The difference of imaging performance in the hybrid NIR/MIR/THz imaging system is also summarized in Table 1.

To highlight the difference in imaging performance among different wavelengths, we visualized a region of a metal blade in the optical chopper [see red square region in Fig. 3(a)]. Figures 3(b)–3(d) show transmission images of the metal blade at $\lambda_{NIR} = 1.6$ µm, $\lambda_{MIR} = 6.3$ µm, and $\lambda_{THz} = 698$ µm, respectively. The image region was 5.2 mm by 5.2 mm, corresponding to 100 pixels by 100 pixels. Therefore, the pixel interval (= 52 µm) is almost the same as the focus spot size in
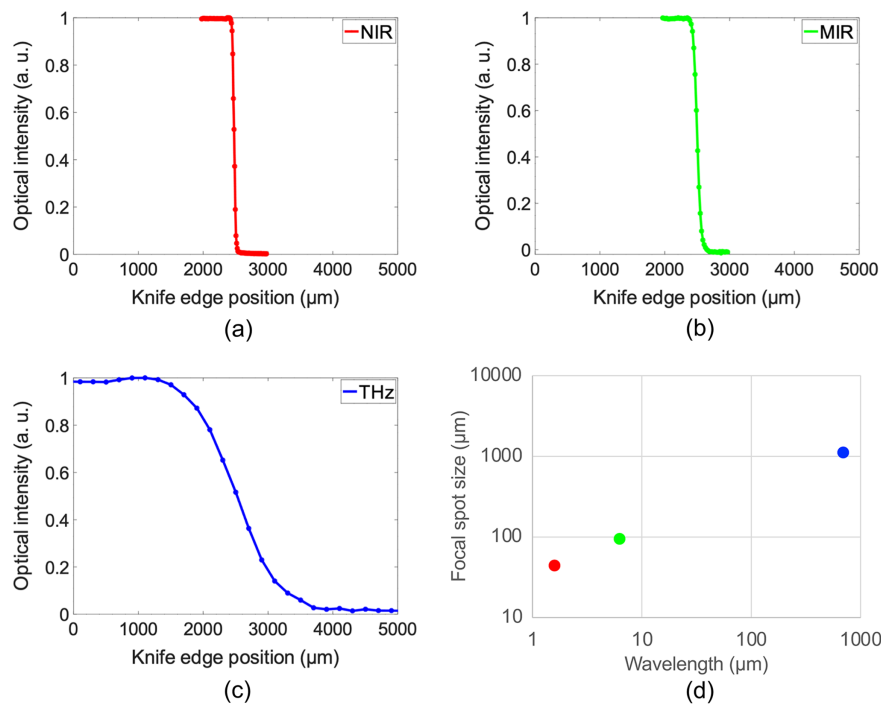
Fig. 2. Knife-edge measurement. Knife-edge profile in (a) NIR imaging, (b) MIR imaging, and (c) THz imaging; (d) comparison of spatial resolution among NIR, MIR, and THz imaging.

Table 1. Imaging Performance of the Hybrid NIR/MIR/THz Imaging System

		NIR Imaging	MIR Imaging	THz Imaging
Wavelength (μm)		1.6	6.3	698
Spatial resolution	Theoretical	22	29	1554
(μm)	Experimental	44	94	1104
DR		5177	55	68
SNR		3976	341	81

Fig. 3. Hybrid optical imaging of a metal blade in an optical chopper. (a) Optical photograph, (b) NIR image, (c) MIR image, and (d) THz image.

the NIR imaging, whereas the pixel interval is smaller than the focus spot in MIR and THz imaging. The NIR image and MIR image show the clear shape of the metal blade with high SNR and similar spatial resolution; the similar spatial resolution between the images well reflects the results in Figs. 2(a) and 2(b). On the other hand, the shape of the metal blade was blurred in THz imaging due to the larger beam waist; however, a moderate SNR was obtained.

B. Internal Structure of Prepaid Transportation Card

The first sample was a prepaid transportation card (size = 54 mm by 85 mm, thickness = 0.75 mm) because nondestructive inspection of plastic products with internal structure is a potential application of our hybrid NIR/MIR/THz imaging system for nondestructive inspection. We performed hybrid imaging of the card sample. Figure 4(a) shows an NIR image (image size = 126 pixels by 402 pixels, image acquisition time = 11,614 s). Internal metal structures were visualized with high spatial resolution despite the considerably low transmission (typically, transmittance of −20 to −30 dB), benefitting from the high sensitivity of the NIR-PD. We confirmed that a square-shaped antenna extended along the card edges and was connected with an IC chip. However, the shadows of the surface printed areas significantly overlapped the image of the internal structures, hampering clear visualization of the internal structure. We acquired no images in MIR imaging due to insufficient transmission (not shown). Figure 4(b) shows a THz image (image size = 112 pixels by 154 pixels, image acquisition time = 5,959 s). In this case, the internal structure of the antenna and integrated circuit chip was well visualized without the influence of surface printed areas. Although the spatial resolution was
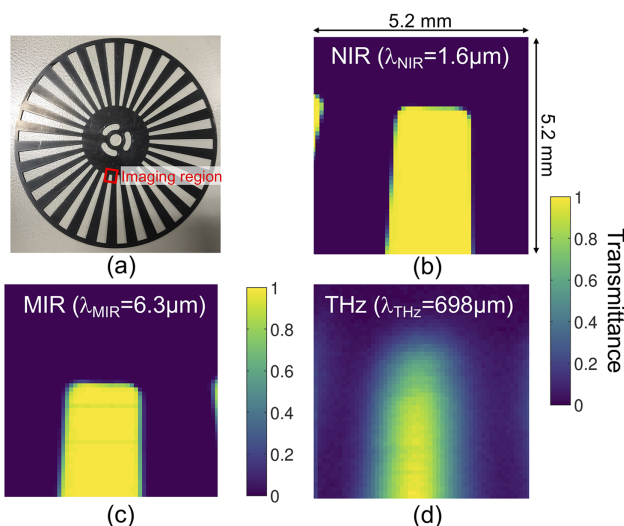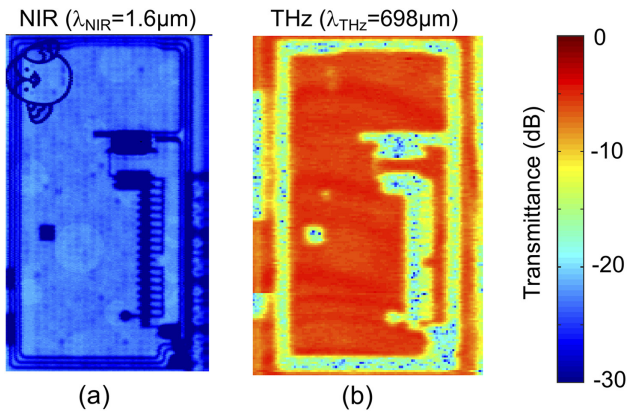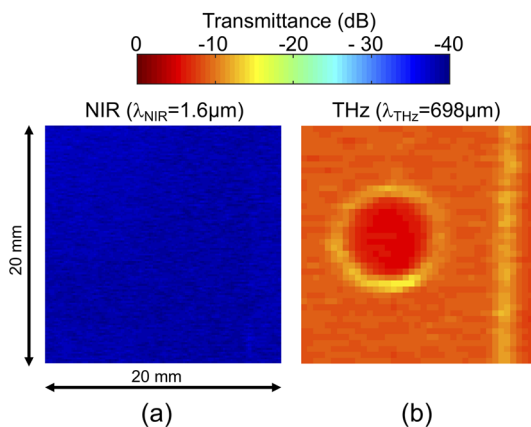
Fig. 4. Hybrid optical imaging of a prepaid transportation card. (a) NIR image and (b) THz image. Sample size is 54 mm width by 85 mm height.

lower than that in NIR imaging, details of internal structures could still be confirmed. In this way, NIR imaging is powerful for nondestructive inspection of card samples having little surface printing with high spatial resolution, whereas THz imaging is useful for nondestructive inspection of card samples having a lot of surface printing with moderate spatial resolution.

C. Air Void in Bulky Resin Material

Detection of void defects is often required in nondestructive inspection of bulky resin material. To investigate the suitability of our hybrid NIR/MIR/THz imaging system for this application, we prepared a black acrylic cube (thickness = 4 mm) with an internal cylindrical hole (hole length = 3 mm, hole diameter = 8 mm). Figure 5(a) shows an NIR image (image size = 20 mm by 20 mm, corresponding to 125 pixels by 125 pixels, image acquisition time = 1,513 s). The NIR image showed no image contrast of air voids because the signal level was below the detection limit in the imaging system, implying strong absorption and/or scattering in the black bulky sample. We acquired no images in MIR imaging (not shown). Figure 5(b) shows a THz image (image size = 20 mm by 20 mm, corresponding to 40 pixels by 40 pixels, image acquisition time = 492 s). The high transmittance of the THz beam in resin material enabled us to clearly visualize the details of a single hole in the sample.
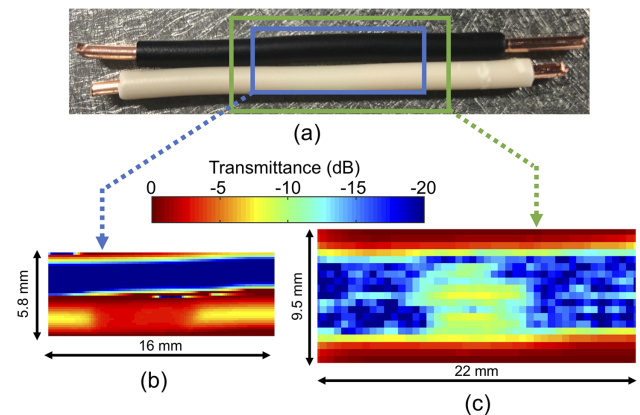
Thus, THz imaging is the only option for nondestructive inspection of bulky resin materials.

D. Internal Break in Power Cable

Power cables are an important electric infrastructure in daily life, and internal breaks directly lead to stoppage of the power supply. To find and repair internal breaks, visual inspection has been widely used; in this case, an inspector finds a part where an internal break or corrosion is suspected, opens the cable coating mechanically, checks the internal metal wire, and covers the wire with a new cable coating after repairing it. However, in this method, the suspected power cable has to be opened whether or not it needs to be repaired. Opening the cable, as well as incomplete covering with the cable coating, may lead to secondary corrosion of the repaired wire due to residual moisture in the cable. Also, such repair work always involves the risk of an electric shock accident during maintenance. Therefore, there is a considerable need for nondestructive inspection of internal breaks in power cables. If polyvinyl chloride (PVC) and polyethylene (PE) used for cable coatings have moderate transmission to NIR, MIR, or a THz beam, our hybrid NIR/MIR/THz imaging system may be a promising candidate for such nondestructive inspection.

To evaluate this, for the samples, we used two usual insulated cables, one covered with a black coating and one covered with a white coating (coating diameter = 3.1 mm, diameter of internal metal wire = 1.6 mm), as shown in Fig. 6(a). To simulate breaks, after opening the cable coatings with a knife, the internal metal wires were cut with a nipper and then were covered with the original coatings again. Figure 6(b) shows an NIR image of the cut cables [see blue square region in Fig. 6(a), image size = 16 mm by 5.8 mm, corresponding to 100 pixels by 36 pixels, image acquisition time = 368 s]. While the cut in the cable with the black coating was not visualized [see upper region of Fig. 6(b)], the cut in the cable with the white coating was visualized with high spatial resolution [see lower region of Fig. 6(b)]. This is mainly due to the difference of the coating material absorptions and indicated that NIR imaging was influenced by the material coloring, although it has potential for nondestructive inspection of breaks in power cables. MIR imaging could not visualize the cuts in the cables (not shown). Figure 6(c) shows a THz image of the cut cables [see green square

Fig. 5. Hybrid optical imaging of air void of bulky resin material. (a) NIR image and (b) THz image.

Fig. 6. Hybrid imaging of internal disconnection of power cable. (a) Optical photograph, (b) NIR image, and (c) THz image.

region in Fig. 6(a), image size = 22 mm by 9.5 mm, pixel size = 44 pixels by 19 pixels, image acquisition time = 320 s]. The cuts in both cables were well visualized in the THz image without any influence of coating material coloring, again highlighting the good material transmission of the THz waves. Although the spatial resolution of the THz image was lower than that of the NIR image, it was still possible to visualize the cut.

4. DISCUSSION

Here we discuss the possibility of NIR, MIR, and THz imaging for nondestructive inspection. While the spatial resolution clearly indicated wavelength dependence based on the diffraction limit (see Figs. 2 and 3), there were large differences in material transmittance among these wavelengths (see Figs. 4–6). First, NIR imaging suffered from relatively low transmittance; however, the combination of a mature high-sensitivity IR detector and the lock-in detection enabled us to visualize the internal structure of the thin sample. Also, we confirmed an interesting feature of NIR imaging: namely, it is sensitive to absorption by printed areas or coloring in the sample. Although the shadows of these areas hindered clear visualization of the internal structure, the feasibility of obtaining an NIR image of both surface and internal structures in specific applications was shown. Second, MIR imaging is an interesting candidate for nondestructive inspection featuring both internal visualization and spectroscopic chemical analysis of the sample. However, MIR imaging could not be applied at all for nondestructive inspection of either thin or thick samples. This was due to the too strong absorption of excessive IR spectral fingerprints. Although use of lock-in detection with a fast MIR detector may improve this situation, one has to consider the risk that the too strong absorption may cause thermal damage to the sample. Third, THz imaging visualized the internal structure of all samples regardless of the material thickness without the influence of absorption by printed areas and coloring in the sample. The only weakness of THz imaging was the slightly blurred image due to the lower spatial resolution. Although the use of higher-frequency THz waves will improve the spatial resolution, it limits the high transmittance through many materials due to lower skin depth. Thus, the compatibility of these imaging modalities differs depending on the sample. The proposed hybrid optical imaging system is a powerful tool for investigating the compatibility and selecting the best imaging modality.

As discussed above, NIR imaging and THz imaging have both merits and demerits: high spatial resolution and low transmittance for the former, and high transmittance and low spatial resolution for the latter. If the merits of both imaging modalities are combined while eliminating their demerits, a hybrid optical imaging technique will become more promising for nondestructive inspection. One potential method of combining the characteristics of different optical imaging methods is image fusion [20]. Image fusion is a process of combining two or more images into a single image, and the resulting single image is more informative and accurate than each original image. For example, IR and visible image fusion has been applied for face recognition [21] and other applications [20]. Also, THz and visible image fusion has been used for hidden object detection [22]. THz and NIR image fusion will combine the merits of THz and NIR imaging and eliminate their demerits, achieving high transmittance with high spatial resolution. A combination of hybrid NIR/THz imaging with an image fusion algorithm is a topic of our future work.

One may consider performing spectroscopy before imaging and then use a suitable wavelength imaging system for optical nondestructive inspection. Unfortunately, spectrometers in NIR, MIR, and THz regions are based on different principles and completely different systems (for example, dispersion-type NIR spectrometers, Fourier-transform MIR spectrometers, and THz time-domain spectrometers). It is not cost-effective to have all of them unless spectroscopic chemical analysis is the main purpose. If just a monochromatic image in the NIR, MIR, or THz region is required for nondestructive inspection, the proposed system is one practical solution.

Also, one may consider that the imaging performance (for example, image acquisition time or portability) of the hybrid imaging system is inferior to that of the existing imaging systems in the NIR, MIR, or THz region. Although that is a fact, we consider that an important role of the hybrid NIR/MIR/THz imaging system is to guess the suitable imaging wavelength prior to the practical imaging. To this end, simultaneous acquisition of NIR, MIR, and THz images by a single system is important. Based on the guess, one can select or construct the practical imaging system in the NIR, MIR, or THz region for practical applications.

5. CONCLUSION

We constructed a hybrid NIR/MIR/THz imaging system for optical nondestructive inspection by using the same imaging optics with different light sources and detectors. NIR imaging indicated the potential to visualize both surface and internal structures of a thin sample with high spatial resolution due to the moderate material transmission and high-sensitivity IR detector. MIR imaging showed difficulty for nondestructive inspection because of the too strong absorption of excessive MIR spectral fingerprints; its use should be limited, not to nondestructive inspection, but to chemical analysis of ultrathin sliced samples. THz imaging showed high promise for nondestructive inspection of both thin and bulky samples, benefitting from the high material transmission. We discussed the possibility of improving the lower spatial resolution of THz imaging by employing image fusion with an NIR image. Although NIR, MIR, and THz images were obtained sequentially by switching light sources and detectors with FMs in this work, use of broadband dichroic mirrors would allow us to obtain the three images simultaneously. As a result, one could easily determine the best imaging wavelength without the need for prior knowledge of the sample properties. Also, a combination of such simultaneously acquired multiple images with image fusion would leads to more informative, accurate, nondestructive inspection by making good use of the light–material interaction characteristics in each wavelength region with image fusion algorithms.

REFERENCES

1. D. E. Bray and D. McBride, *Nondestructive Testing Techniques* (Wiley, 1992).
2. P. J. Withers and M. Preuss, "Fatigue and damage in structural materials studied by x-ray tomography," Annu. Rev. Mater. Res. **42**, 81–103 (2012).
3. J. R. Rygg, O. S. Jones, J. E. Field, M. A. Barrios, L. R. Benedetti, G. W. Collins, D. C. Eder, M. J. Edwards, J. L. Kline, J. J. Kroll, O. L. Landen, T. Ma, A. Pak, J. L. Peterson, K. Raman, R. P. J. Town, and D. K. Bradley, "2D x-ray radiography of imploding capsules at the national ignition facility," Phys. Rev. Lett. **112**, 195001 (2014).
4. M. T. M. Khairi, M. A. Md Yunus, M. Faramarzi, G. P. Sean, J. Pusppanathan, and A. Abid, "Ultrasound computed tomography for material inspection: principles, design and applications," Measurement **146**, 490–523 (2019).
5. M. H. Skjelvareid, Y. Birkelund, and Y. Larsen, "Internal pipeline inspection using virtual source synthetic aperture ultrasound imaging," NDT&E Int. **54**, 151–158 (2013).
6. J. M. Chalmers and P. R. Griffiths, *Handbook of Vibrational Spectroscopy* (Wiley, 2002).
7. M. Manley, "Near-infrared spectroscopy and hyperspectral imaging: non-destructive analysis of biological materials," Chem. Soc. Rev. **43**, 8200–8214 (2014).
8. D. F. Barbin, G. ElMasry, D.-W. Sun, and P. Allen, "Non-destructive determination of chemical composition in intact and minced pork using near-infrared hyperspectral imaging," Food Chem. **138**, 1162–1171 (2013).
9. B. Van Eerdenbrugh, M. Lo, K. Kjoller, C. Marcott, and L. S. Taylor, "Nanoscale mid-infrared imaging of phase separation in a drug–polymer blend," J. Pharm. Sci. **101**, 2066–2073 (2012).
10. K. Haase, N. Kröger-Lui, A. Pucci, A. Schönhals, and W. Petrich, "Real-time mid-infrared imaging of living microorganisms," J. Biophoton. **9**, 61–66 (2016).
11. D. M. Mittleman, "Twenty years of terahertz imaging," Opt. Express **26**, 9417–9431 (2018).
12. S. Zhong, "Progress in terahertz nondestructive testing: a review," Front. Mech. Eng. **14**, 273–281 (2019).
13. C. Jördens, M. Scheller, S. Wietzke, D. Romeike, C. Jansen, T. Zentgraf, K. Wiesauer, V. Reisecker, and M. Koch, "Terahertz spectroscopy to study the orientation of glass fibres in reinforced plastics," Compos. Sci. Technol. **70**, 472–477 (2010).
14. D.-D. Zhang, J.-J. Ren, J. Gu, L.-J. Li, J.-Y. Zhang, W.-H. Xiong, Y.-F. Zhong, and T.-Y. Zhou, "Nondestructive testing of bonding defects in multilayered ceramic matrix composites using THz time domain spectroscopy and imaging," Compos. Struct. **251**, 112624 (2020).
15. K. Krügener, E.-M. Stübling, R. Jachim, B. Kietz, M. Koch, and W. Viöl, "THz tomography for detecting damages on wood caused by insects," Appl. Opt. **58**, 6063–6066 (2019).
16. M. Kato, S. R. Tripathi, K. Murate, K. Imayama, and K. Kawase, "Non-destructive drug inspection in covering materials using a terahertz spectral imaging system with injection-seeded terahertz parametric generation and detection," Opt. Express **24**, 6425–6432 (2016).
17. K. Fukunaga and I. Hosako, "Innovative non-invasive analysis techniques for cultural heritage using terahertz technology," C. R. Physique **11**, 519–526 (2010).
18. M. Asada, S. Suzuki, and N. Kishimoto, "Resonant tunneling diodes for sub-terahertz and terahertz oscillators," Jpn. J. Appl. Phys. **47**, 4375–4384 (2008).
19. S. Suzuki, M. Asada, A. Teranishi, H. Sugiyama, and H. Yokoyama, "Fundamental oscillation of resonant tunneling diodes above 1 THz at room temperature," Appl. Phys. Lett. **97**, 242102 (2010).
20. J. Ma, Y. Ma, and C. Li, "Infrared and visible image fusion methods and applications: a survey," Inf. Fusion **45**, 153–178 (2019).
21. R. Singh, M. Vatsa, and A. Noore, "Integrated multilevel image fusion and match score fusion of visible and infrared face images for robust face recognition," Pattern Recogn. **41**, 880–893 (2008).
22. M. Kowalski, N. Palka, M. Piszczek, and M. Szustakowski, "Hidden object detection system based on fusion of THz and VIS images," Acta Phys. Pol. A **124**, 490–493 (2013).